Durham Research Online

Additional information:

The twisted dark matter halo of the Milky Way

Shi Shao [ORCID],[1][*] Marius Cautun [ORCID],[1,2] Alis Deason [ORCID][1] and Carlos S. Frenk[1]

[1]*Institute for Computational Cosmology, Department of Physics, Durham University, South Road, Durham DH1 3LE, UK*
[2]*Leiden Observatory, Leiden University, PO Box 9513, NL-2300 RA Leiden, the Netherlands*

ABSTRACT

We analyse systems analogous to the Milky Way (MW) in the EAGLE cosmological hydrodynamics simulation in order to deduce the likely structure of the MW's dark matter (DM) halo. We identify MW mass haloes in the simulation whose satellite galaxies have similar kinematics and spatial distribution to those of the bright satellites of the MW, specifically systems in which the majority of the satellites (8 out of 11) have nearly coplanar orbits that are also perpendicular to the central stellar disc. We find that the normal to the common orbital plane of the coplanar satellites is well aligned with the minor axis of the host DM halo, with a median misalignment angle of only $17.3°$. Based on this result, we infer that the minor axis of the Galactic DM halo points towards $(l, b) = (182°, -2°)$, with an angular uncertainty at the 68 and 95 percentile confidence levels of $22°$ and $43°$, respectively. Thus, the inferred minor axis of the MW halo lies in the plane of the stellar disc. The halo, however, is not homologous and its flattening and orientation vary with radius. The inner parts of the halo are rounder than the outer parts and well aligned with the stellar disc (that is the minor axis of the halo is perpendicular to the disc). Further out, the halo twists and the minor axis changes direction by $90°$. This twist occurs over a very narrow radial range and reflects variations in the filamentary network along which mass was accreted into the MW.

Key words: methods: numerical – galaxies: haloes – galaxies: kinematics and dynamics.

1 INTRODUCTION

One of the fundamental predictions of the standard cosmological model (ΛCDM) is that galaxies are surrounded by extended distributions of dark matter (DM) – the DM haloes (Davis et al. 1985). These are essential for galaxy formation since they provide the gravitational potential wells within which gas is able to cool, condense, and form stars (White & Rees 1978; White & Frenk 1991; for a review, see Somerville & Davé 2015). DM haloes are the end product of the anisotropic gravitational collapse of non-dissipative matter and thus have highly non-spherical shapes (see Frenk & White 2012; Zavala & Frenk 2019, for recent reviews). Measuring the DM mass distribution and, in particular, the shape of haloes, provides a crucial test of the standard cosmological model and could reveal the nature of DM or rule out alternative cosmological theories. Here, we investigate how the Milky Way (MW) disc of satellite galaxies can be used to infer the orientation and aspects of the formation history of the Galactic DM halo.

Our galaxy offers a prime test bed for characterizing the DM distribution around galaxies. Numerous studies have focused on determining the mass and radial density profile of the Galactic DM halo by analysing the dynamics of halo stars, globular clusters, and satellite galaxies (e.g. Xue et al. 2008; Deason et al. 2012; Callingham et al. 2019; Eadie & Jurić 2019; Posti & Helmi 2019; Watkins et al. 2019) or simply the number and other properties of the satellites (e.g. Busha et al. 2011; Cautun et al. 2014b). By contrast,

far fewer studies have attempted to infer the shape and orientation of the Galactic DM halo, which, in part, is a manifestation of the difficulties inherent in such a task.

In ΛCDM, DM haloes have a range of shapes and can be described as ellipsoidal mass distributions, with a preference for prolate over oblate shapes (e.g. Frenk et al. 1988; Dubinski & Carlberg 1991; Warren et al. 1992; Jing & Suto 2002; Allgood et al. 2006; Bett et al. 2007; Hayashi, Navarro & Springel 2007; Schneider, Frenk & Cole 2012). The axial ratios and orientations of the mass ellipsoids vary as a function of distance from the halo centre and contain imprints of the past growth history of the halo, with each shell retaining memory of the mass accretion properties at the time when it collapsed (e.g. Wechsler et al. 2002; Vera-Ciro et al. 2011; Wang et al. 2011; Ludlow et al. 2013). Galaxy formation simulations have shown that the mass distribution within haloes can be significantly affected by the baryonic distribution and, in particular, by the orientation of the central galaxy. In the very inner few tens of kiloparsecs, baryonic matter can dominate the potential and cause the DM distribution to become less aspherical than predicted by simulations of dissipationless collapse and well aligned with the central galaxy (e.g. Abadi et al. 2003; Bailin et al. 2005; Bryan et al. 2013; Tenneti et al. 2014, 2015; Velliscig et al. 2015a,b; Shao et al. 2016; Chua et al. 2019). At large distances, the potential of the baryonic component is subdominant and the DM haloes retain a similar shape and orientation to those found in DM-only simulations.

Since DM cannot yet be observed directly, the shape and orientation of haloes can only be inferred from gravitational effects and correlations with visible tracers. The wealth of dynamical tracers around the MW and, in particular, the exquisite quality and sheer size of the

Gaia data set (Gaia Collaboration 2018) has led to the development of a multitude of methods for studying the Galactic DM halo (see Wang et al. 2019, for a recent review), including inferring halo shapes from the properties of stellar streams (e.g. Sanders & Binney 2013; Price-Whelan et al. 2014; Bowden, Belokurov & Evans 2015; Bovy et al. 2016; Malhan & Ibata 2019), the stellar halo (e.g. Bowden, Evans & Williams 2016; Wegg, Gerhard & Bieth 2019), and hypervelocity stars (e.g. Gnedin et al. 2005; Contigiani, Rossi & Marchetti 2019).

Many studies of the shape of the Galactic DM halo are based on the tidal stream of the Sagittarius dwarf, which traces the Galactic potential within ∼100 kpc, and argue for a highly flattened halo that is oriented perpendicular to the MW disc (Helmi 2004; Johnston, Law & Majewski 2005; Law & Majewski 2010; Deg & Widrow 2013). The best-fitting Law & Majewski (2010) model has an oblate halo, with axial ratios, $\langle c/a \rangle = 0.72$ and $\langle b/a \rangle = 0.99$, flatter than the typical halo in ΛCDM (Hayashi et al. 2007); furthermore, its alignment with the MW disc does not form a stable configuration (Debattista et al. 2013). Motivated by these inconsistencies, Vera-Ciro & Helmi (2013) improved the model by allowing the shape and orientation of the DM halo to vary with radius, from a mildly flattened halo in the inner ∼20 kpc (which is also supported by GC; Posti & Helmi 2019) to the Law & Majewski configuration at larger distances. Vera-Ciro & Helmi (2013) and Gómez et al. (2015) have highlighted that the Large Magellanic Cloud (LMC), which is thought to be very massive (Peñarrubia et al. 2016; Laporte et al. 2018; Shao et al. 2018b; Cautun et al. 2019), can induce significant dynamical perturbations to the orbit of the Sagittarius tidal stream as well as other streams (e.g. the Tucana III stream; Erkal et al. 2018), thus further complicating the modelling of the Galactic halo potential.

Most studies of halo shape and orientation are restricted to the inner DM halo (<100 kpc) since this is where the majority of dynamical tracers are found. At larger distances, little is known about the shape of the halo and most conclusions are deduced from statistical correlations. For instance, the central galaxy seems well aligned with the inner halo and it has been argued that this alignment is preserved, although with some degradation, all the way to the virial radius, allowing the orientation of the halo minor axis to be inferred within a median angle of ∼33° (e.g. Bailin et al. 2005; Tenneti et al. 2015; Velliscig et al. 2015a; Shao et al. 2016).

Satellite galaxies are preferentially accreted along filaments (Libeskind et al. 2005, 2014; Shao et al. 2018a) – in the same directions as mass is accreted on to haloes – and thus the satellites also trace the DM halo including its large-scale orientation (Libeskind et al. 2007; Shao et al. 2016). However, in the MW the satellites are found in a plane perpendicular to the Galactic disc (e.g. Kunkel & Demers 1976; Lynden-Bell 1976, 1982; Kroupa, Theis & Boily 2005), and this suggests a very different halo orientation from that inferred from the orientation of the MW disc. Shao et al. (2016) studied configurations in which the satellites are found in a plane perpendicular to the central disc and have found that, in this case, the DM halo is poorly aligned with the central galaxy. Thus, we cannot use the MW stellar disc to predict the orientation of the Galactic halo.

In this paper, we use the rotating disc of classical dwarf galaxies in the MW to infer possible formation histories and configurations of the Galactic DM halo. The paper is motivated by the results of Shao, Cautun & Frenk (2019) who showed that out of the 11 MW classical dwarfs, 8 orbit in nearly the same plane (see also Pawlowski, Kroupa & Jerjen 2013) – specifically the orbital poles of those 8 satellites are enclosed within a 22° opening angle. Shao et al. (2019) showed that MW-like rotating planes of satellites in ΛCDM are a consequence of highly anisotropic accretion and, most importantly for this study, of the torques exerted by the host halo which tilt the satellite orbits

on to the host halo's equatorial plane. This suggests that the satellite orbital plane should be a good indicator of halo orientation, which is one of the main questions we investigate here.

We proceed by identifying in the EAGLE galaxy formation simulation (Schaye et al. 2015) satellite systems similar to the MW, in which 8 out of the brightest 11 satellites orbit in nearly the same plane. The common orbital plane is very nearly perpendicular to the minor axis of the host DM halo and thus can be used to predict the orientation of the Galactic DM halo. We then identify EAGLE MW mass systems that have a rotating plane of satellites that is perpendicular to their central galaxy, as found in our Galaxy, and perform an in-depth study of such systems. The goal is to understand the processes that give rise to the perpendicular configuration between satellites and central galaxy and what this can tell us about the formation history of the Galactic DM halo.

The paper is organized as follows. In Section 2, we review the simulations used in this work and describe our sample selection; in Section 3, we analyse the DM halo properties of systems that have satellite distributions similar to our own galaxy; then in Section 4, we study the formation history of five MW mass haloes that are very similar to the MW; we conclude with a short summary and discussion in Section 5.

2 SIMULATION AND SAMPLE SELECTION

We analyse the main cosmological hydrodynamics simulation (labelled Ref-L0100N1504) of the EAGLE project (Crain et al. 2015; Schaye et al. 2015). The simulation follows the evolution of a periodic cube of sidelength 100 Mpc with 1504^3 DM particles and an initially equal number of gas particles. The DM particle mass is 9.7×10^6 M$_\odot$ and the initial gas particle mass is 1.8×10^6 M$_\odot$. The simulation assumes the *Planck* cosmological parameters (Planck Collaboration XVI 2014): $\Omega_m = 0.307$, $\Omega_b = 0.04825$, $\Omega_\Lambda = 0.693$, $h = 0.6777$, $\sigma_8 = 0.8288$, and $n_s = 0.9611$.

The simulation was performed with a modified version of the GADGET code (Springel 2005), which includes state-of-the-art smooth particle hydrodynamics and subgrid models for baryonic processes such as element-by-element gas cooling, star formation, metal production, stellar winds, and stellar and black hole feedback. The EAGLE subgrid models were calibrated to reproduce three present-day observables: the stellar mass function, the dependence of galaxy sizes on stellar mass, and the normalization of the relation between supermassive black hole mass and host galaxy mass. For a more detailed description, please see Schaye et al. (2015) and Crain et al. (2015).

To identify analogues of the MW satellite system, we make use of the $z = 0$ EAGLE halo and galaxy catalogue (McAlpine et al. 2016). The haloes and galaxies correspond to gravitationally bound substructures identified by the SUBFIND code (Springel, Yoshida & White 2001; Dolag et al. 2009) applied to the full mass distribution (DM, gas, and stars). The main haloes are characterized by the mass, M_{200}, and radius, R_{200}, that define an enclosed spherical overdensity of 200 times the critical density. The position of each galaxy, both centrals and satellites, is given by their most bound particle. We also study the formation history of several individual systems, for which we use the EAGLE galaxy merger trees (Qu et al. 2017) built from over 200 snapshots (roughly one every 70 Myr).

2.1 Sample selection

We wish to work with a cosmologically representative sample of satellite systems of similar stellar masses to the classical dwarfs that
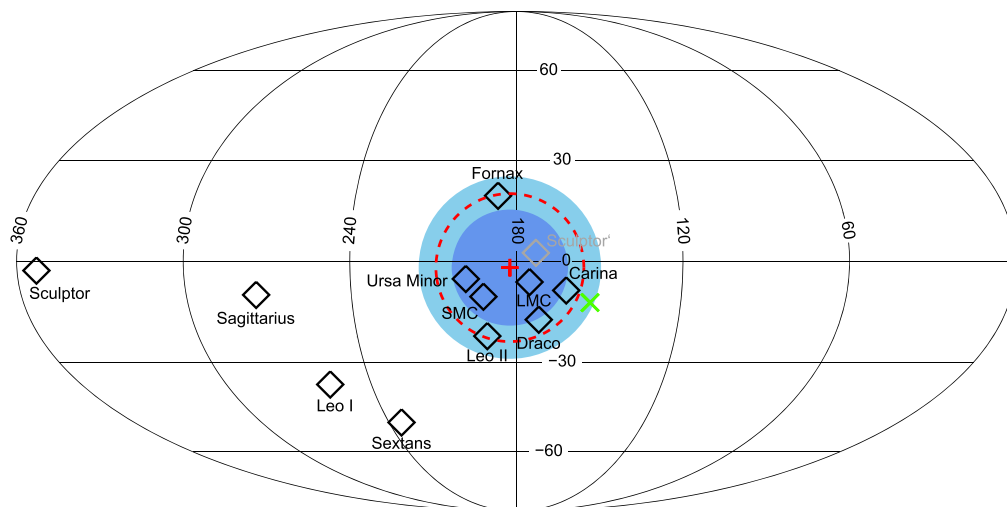
Figure 1. Aitoff projection of the orbital poles of the classical satellites of the MW. Each black rhombus corresponds to the orbital pole of a classical dwarf in Galactic longitude, l, and latitude, b. Shao et al. (2019) have shown that 8 out of the 11 classical satellites have highly clustered orbital poles that are contained within a $22°$ opening angle (red dashed circle) around the direction $(l, b) = (182°, -2°)$ (red cross symbol). Out of the eight satellites with coplanar orbits, Sculptor is counter-rotating, and, to emphasize that its orbit is in the same plane, the grey rhombus shows its position after flipping its orbital pole. The green x shows the minor axis of the spatial distribution of satellites. In this paper, we show that the minor axis of the Galactic DM halo likely points towards the red cross symbol. The two coloured regions show, respectively, the 50 and 75 percentile confidence interval for our determination of the orientation of the halo's minor axis.

orbit around the MW. We use the sample studied by Shao et al. (2016) that consists of 1080 EAGLE galaxies selected according to the following criteria: (i) they are the central galaxy in a halo of mass $M_{200} \in [0.3, 3] \times 10^{12}$ M$_\odot$ and (ii) they have at least 11 luminous satellites within a distance of 300 kpc from the central galaxy. We define luminous satellites as subhaloes with at least one associated stellar particle, corresponding to objects of stellar mass larger than $\sim 1 \times 10^6$ M$_\odot$. If there are more than 11 satellites within the chosen distance, we only consider the 11 with the highest stellar mass.

We further require that the MW-like analogues be isolated, that is that they have no neighbours more massive than themselves within a distance of 600 kpc. This isolation criterion is not very strict and, for example, the MW would fulfil it since Andromeda is $\sim$800 kpc away (McConnachie 2012). The median halo mass of our sample is 1.2×10^{12} M$_\odot$ (see fig. A1 of Shao et al. 2016 for the exact halo mass distribution), which is in good agreement with recent determinations of the MW halo mass (see e.g. Patel et al. 2018; Callingham et al. 2019; Deason et al. 2019; Cautun et al. 2020; and fig. 5 in the Wang et al. 2019 review). We have not applied a morphological selection, so our sample of MW-like galaxies contains the full range of morphologies produced in the EAGLE model (Trayford et al. 2015; Correa et al. 2017).

The radial distribution of satellites in our EAGLE MW mass sample is slightly less concentrated than the distribution of the MW classical satellites (see also Yniguez et al. 2014; Carlsten et al. 2020). This is likely due to substructures that are prematurely disrupted in the simulation (Bose et al. 2020). These absent satellites should typically be found in the inner 100 kpc of the halo and, comparing to the radial distribution of Bose et al., we estimate that our sample is lacking, on average, 1–2 such satellites per system. We expect that including these additional satellites in future studies based on much higher resolution simulations would have minimal impact on our conclusions. Most satellites are accreted along a plane (Shao et al. 2019), so the inner satellites have, on average, the same distribution of orbital planes as the outer ones. Furthermore, as we shall discuss shortly, our study concerns planes defined by 8 out of the 11 brightest

satellites that have the most coplanar orbits. This definition results in planes that are robust to replacing one of the satellites since, even if the newly added object had a very different orbital plane, it would not be included in our subset of satellites with coplanar orbits and thus would not have a large impact on the plane of satellite galaxies.

2.2 Identifying MW-like rotating planes of satellites

We identify satellites with coplanar orbits using the method introduced by Shao et al. (2019). The goal is to find satellite distributions similar to that in the MW, where 8 out of the 11 classical satellites orbit in roughly the same plane.[1] This is illustrated in Fig. 1, which shows the orbital poles of the classical satellites. Shao et al. (2019) have quantified the degree of coplanarity of the orbits by the minimum opening angle, α_8, needed to enclose the orbital poles of the 8 satellites whose orbits are closest to a single plane. For the MW, $\alpha_8 = 22°$, shown in Fig. 1 as the red dashed circle centred on $(l, b) = (182°, -2°)$.

For each MW mass galaxy in our sample, we identify the subset of eight satellites whose orbits exhibit the highest degree of coplanarity as follows. We first generate 10^4 uniformly distributed directions on the unit sphere and, for each direction, we find the minimum opening angle that includes the orbital poles of eight satellites. We then select the direction with the smallest opening angle. We denote the smallest opening angle as α_8; its corresponding direction is the normal to the *common orbital plane* in which the eight satellites orbit, which we denote as $\hat{n}_{orbit}$.

The distribution of α_8 opening angles for ΛCDM MW mass haloes can be found in fig. 4 of Shao et al. (2019). We emphasize that very few (only 6 out of 1080) EAGLE haloes have α_8 values as low

---

[1]The choice of 8 out of 11 satellites is explained in fig. 3 of Shao et al., which shows that a subset of eight classical MW dwarfs have highly coplanar orbits that stand out when compared to either typical ΛCDM systems or isotropic distributions of orbits.
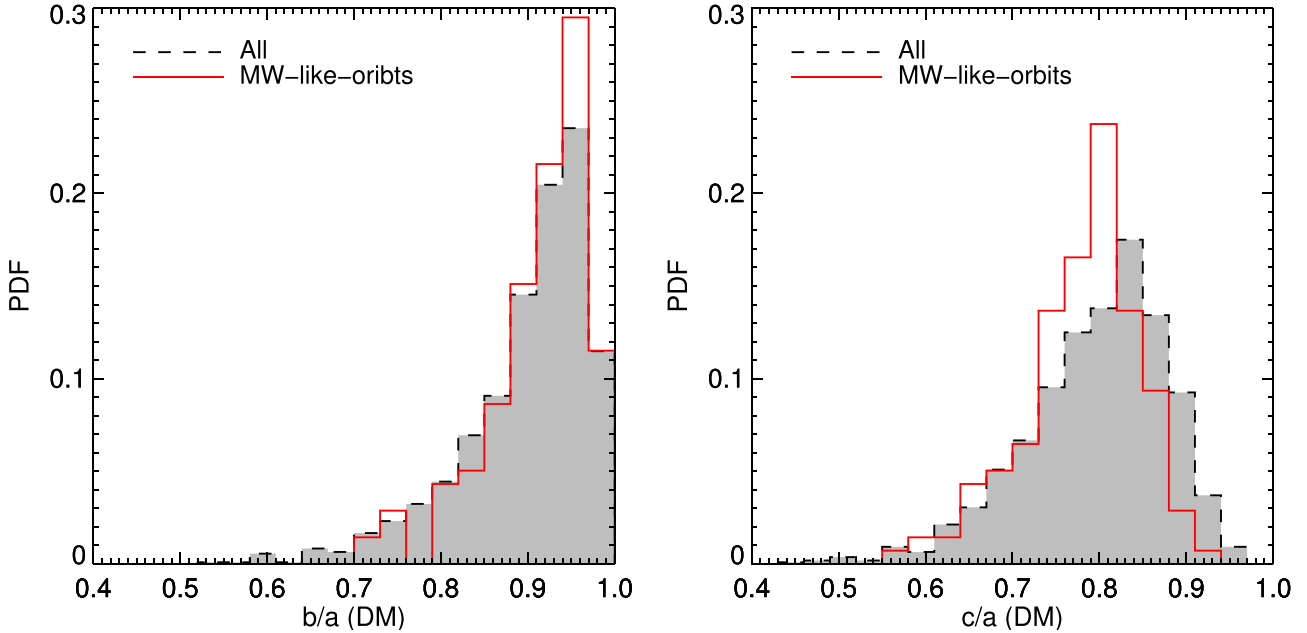
Figure 2. The distribution of axial ratios, *b/a* (left-hand panel) and *c/a* (right-hand panel) of the shape of the entire DM halo, that is all the DM particles within R_{200}. The dashed line shows the result for all MW mass haloes, while the red solid line corresponds to the sample of *MW-like-orbit* systems. We find with a high statistical confidence that the Galactic DM halo is more flattened (smaller *c/a*) than the average ΛCDM halo. Also, we find hints that the MW halo is more likely to have $a \approx b$ (i.e. more oblate) than the typical expectation, however, due to the small sample size we cannot rule out that this difference is due to statistical fluctuations (see main text for details).

as the MW. The rarity of such MW-like systems is somewhat by construction, because we want to study a feature of the MW satellite distribution that is uncommon when compared to the typical ΛCDM halo. In fact, a considerable fraction of ΛCDM haloes have rotating planes of satellites; however, each plane is different suggesting that the planes encode information about the evolution of that particular system (Cautun et al. 2015b). To obtain a reasonable number of EAGLE satellite systems with orbits similar to those of the MW system, we define *MW-like-orbit* systems as those with opening angles, $\alpha_8 < 35°$. There are ∼140 EAGLE haloes (13 per cent of the sample) that fulfil this selection criterion.

3 THE DM HALOES OF MW-LIKE-ORBIT SYSTEMS

We refer to the DM haloes of galactic mass systems in which 8 out of the brightest 11 satellite galaxies orbit in a narrow plane as *MW-like-orbit* systems We study the shape of the DM haloes and their orientation relative to the plane of satellite, the central galaxy, and the large-scale structure (LSS) surrounding these systems.

3.1 The DM halo shape

We characterize the shape of a DM halo by its mass tensor,

$$I_{ij} \equiv \sum_{k=1}^{N} x_{k,i}\, x_{k,j}\,, \tag{1}$$

where the sum is over the DM particles found within the halo radius, R_{200}. The quantity $x_{k,i}$ denotes the *i*-th component ($i = 1, 2, 3$) of the position vector associated with the *k*-th DM particle, measured with respect to the halo centre. The shape and the orientation are determined by the eigenvalues, λ_i ($\lambda_1 \geq \lambda_2 \geq \lambda_3$), and the

eigenvectors, $\hat{e}_i$, of the mass tensor. The major, intermediate, and minor axes of the corresponding ellipsoid are given by $a = \sqrt{\lambda_1}$, $b = \sqrt{\lambda_2}$, and $c = \sqrt{\lambda_3}$, respectively, and their orientation is given by $\hat{e}_1, \hat{e}_2$, and $\hat{e}_3$. We obtain the same eigenvalues and eigenvectors if, instead, we define the halo shape using the moment of inertia tensor (Bett et al. 2007).

When calculating halo shapes, we use all the DM particles enclosed within R_{200} (for the full halo), or within a fixed radial distance when calculating the shape as a function of radius. We prefer this choice compared to alternatives such as removing bound substructures, since it is closer to what can be done in observations. Observations measure the shape of the total gravitational potential and, with a few exceptions such as the LMC, it is very difficult to isolate the contribution of each substructure to the total potential. In general, the shape measurement is mostly insensitive to substructures, except for a small number of hosts that contain massive satellites (Bett et al. 2007).

We describe the halo shape by the intermediate-to-major, *b/a*, and minor-to-major, *c/a*, axial ratios, which characterize the degree of halo flattening. The two axial ratios are shown in Fig. 2, where we compare the flattening of the full sample of MW mass systems to that of *MW-like-orbit* ones. The full sample is characterized by preferentially prolate haloes ($a > b \approx c$) with a median flattening of $b/a \sim 0.9$ and $c/a \sim 0.8$, in good agreement with previous studies (e.g. Frenk et al. 1988; Bett et al. 2007; Schneider et al. 2012; Shao et al. 2016).

The haloes of the *MW-like-orbits* sample show systematic differences compared to the full sample. Since the *MW-like-orbits* sample is rather small, only 139 objects, we assess the statistical significance of any observed differences using the Kolmogorov–Smirnov (KS) test. First, the *MW-like-orbit* haloes have *b/a* axial ratios that are somewhat larger than that of the full sample. However, the effect is rather small and a KS test indicates that the difference
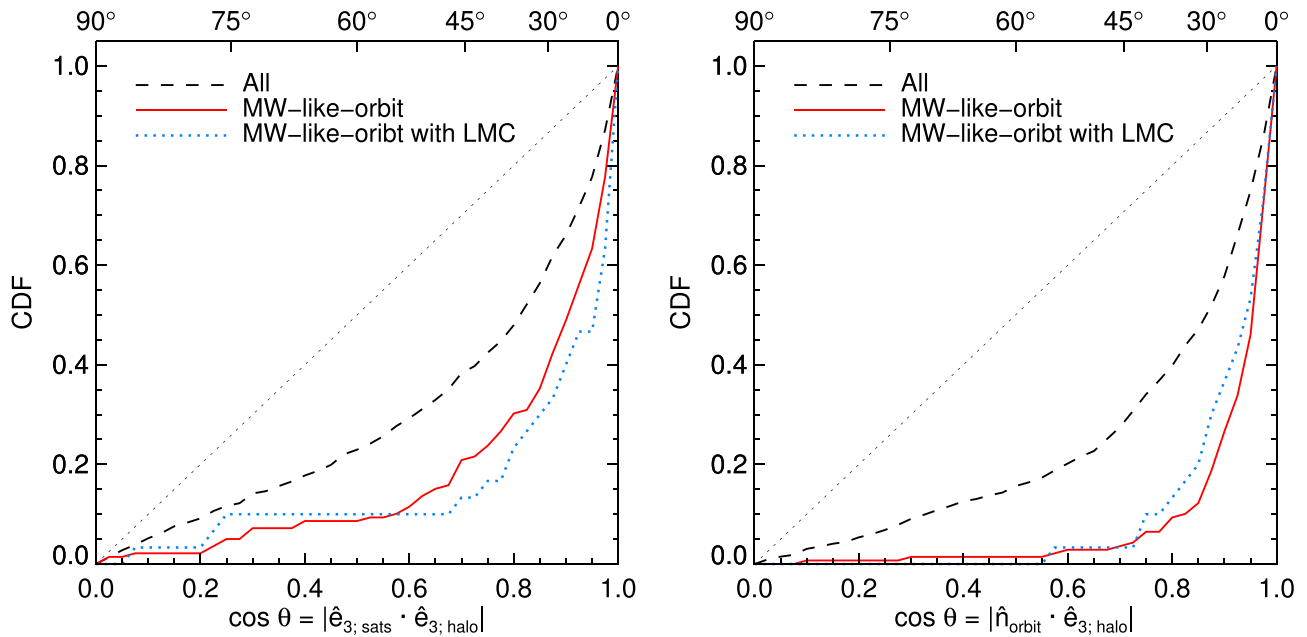
Figure 3. Left-hand panel: The CDF of the alignment angle, $\cos\theta$, between the minor axis of the satellite system and the minor axis of the DM halo in the EAGLE simulation. The three lines correspond to: all MW mass haloes (dashed), *MW-like-orbit* haloes (solid red), and *MW-like-orbit* haloes with an LMC mass dwarf satellite (dotted blue). Right-hand panel: As the left-hand panel, but for the alignment angle between the normal to the common orbital plane of the satellites and the minor axis of the DM halo. In both panels, the dotted diagonal line shows the CDF for the no-alignment case. Both the minor axis of the satellite system and the normal to the common preferential orbital plane are aligned with the halo minor axis; however, the latter shows a much tighter alignment. Thus, the plane in which most satellites orbit is a very good indicator of the DM halo minor axis and especially for systems that have *MW-like-orbit* planes.

is not statistically significant (i.e. there is a $p = 0.27$ probability that both samples follow the same distribution). Secondly, the *MW-like-orbit* haloes have c/a axial ratios that are systematically smaller than that of the full sample. This result is statistically robust, with a KS test probability of $p = 3 \times 10^{-4}$ that the observed difference is due to statistical fluctuations. Thus, the orbital clustering of the MW classical satellites indicates that the Galactic DM halo is systematically flatter (i.e. smaller c/a ratio) than the typical ΛCDM halo.

The haloes of *MW-like-orbit* systems are flattened because they experience a higher degree of anisotropic accretion, especially planar infall, than the average ΛCDM halo. This is illustrated in fig. 7 of Shao et al. (2019), where we showed that systems with many coplanar satellite orbits had a higher degree of anisotropic infall (see also Libeskind et al. 2005; Deason et al. 2011; Lovell et al. 2011; Kang & Wang 2015; Shao et al. 2018a). The preferential infall plane is responsible for the coherent orbital planes of satellites as well as for the flattening of the DM halo, with the equatorial plane of the halo being aligned with the anisotropic infall plane (e.g. Hahn et al. 2007; Ganeshaiah Veena et al. 2018, 2019).

3.2 The orientation of the DM halo with respect to the satellite distribution

We now study the extent to which the satellite distribution can constrain the orientation of the DM halo. To this aim, Fig. 3 shows the alignment of the satellite distribution with the minor axis of the DM halo.

To begin with, we follow the standard approach in the literature and define the orientation as the direction of the minor axis of the satellite system (e.g. Kroupa et al. 2005; Libeskind et al. 2005; Deason et al. 2011). This is calculated from the mass tensor of the distribution

using equation (1) applied to the 11 brightest satellites of each system. The resulting orientation of the minor axis of the MW classical satellites is shown as the green cross symbol in Fig. 1. Applying the same procedure to the EAGLE systems, we find a moderate alignment between the minor axis of the satellite distribution and the minor axis of the DM halo, with a median alignment angle of $35.7°$. The subset of systems with *MW-like-orbits* show a better alignment between their satellite distribution and DM halo, with a median alignment angle of $24.8°$ (see Fig. 3 and Table 1).

The MW has recently accreted a massive satellite, the LMC, that could potentially affect the orientation of its DM halo (e.g. Garavito-Camargo et al. 2019) and satellite orbits (e.g. Gómez et al. 2015; Patel et al. 2020), in addition to bringing in its own satellites. To study the potential effect of the LMC, we have further identified the subset of *MW-like-orbits* system that also have an LMC mass dwarf satellite. We define an LMC mass analogue as any satellite located less than 150 kpc from the central galaxy and with stellar mass greater than 1×10^9 M$_\odot$ (van der Marel et al. 2002; McConnachie 2012; Shao et al. 2018b). We find that $\sim$20 per cent of the sample (30 out of 139) have an LMC mass dwarf; we find roughly the same prevalence of LMC mass satellites for the full population of MW mass systems. The alignment of *MW-like-orbit* systems that have an LMC mass satellite is similar to that of the *MW-like-orbits* subset, with differences consistent with stochastic effects due to the small number of systems with LMC mass satellites.

The orientation of the satellite distribution can also be defined as the normal, $\hat{n}_{\rm orbit}$, to the common orbital plane of the eight satellites with the most coplanar orbits (see Section 2.2). The $\hat{n}_{\rm orbit}$ direction is robust, varying only slowly with time. This is in contrast to the minor axis of the satellite distribution, which can vary rapidly with time and whose orientation is especially sensitive to the farthest most satellites (e.g. Buck, Dutton & Macciò 2016; Lipnicky & Chakrabarti 2017;

Table 1. The median alignment angles between the satellite distribution of MW mass galaxies and their DM haloes, central galaxies, and surrounding LSS. We provide results for three samples of MW mass systems: all (second column), those with *MW-like-orbits* (third column), and those with *MW-like-orbits* that also have an LMC mass dwarf satellite (fourth column). We provide values for the median angle and the 68 percentile confidence interval with which we can determine the median.

Alignment type	Sample		
	All	*MW-like-orbits*	*MW-like-orbits* with LMC mass satellite
(1) $\theta_{\text{sats–halo}}$	$35.7^{+0.9}_{-0.8}$	$24.8^{+2.9}_{-1.4}$	$16.2^{+8.1}_{-2.9}$
(2) $\theta_{\text{orbit–halo}}$	$30.2^{+0.7}_{-1.1}$	$17.3^{+1.1}_{-0.6}$	$18.7^{+3.9}_{-3.9}$
(3) $\theta_{\text{orbit–cen}}$	$41.3^{+1.5}_{-0.7}$	$24.8^{+1.4}_{-0.9}$	$36.2^{+7.5}_{-10.1}$
(4) $\theta_{\text{orbit–LSS}}$	$51.6^{+1.5}_{-1.6}$	$45.1^{+2.0}_{-4.5}$	$37.9^{+7.2}_{-2.6}$

Notes. (1) The median angle between the minor axis of the satellite distribution, $\hat{e}_{3;\,\text{sats}}$, and the minor axis of the DM halo, $\hat{e}_{3;\,\text{halo}}$.
(2) The median angle between the normal to the common orbital plane of the satellites, $\hat{n}_{\text{orbit}}$, and the minor axis of the DM halo, $\hat{e}_{3;\,\text{halo}}$.
(3) The median angle between the normal to the common orbital plane of the satellites, $\hat{n}_{\text{orbit}}$, and the minor axis of the central galaxy, $\hat{e}_{3;\,\text{cen}}$.
(4) The median angle between the normal to the common orbital plane of the satellites, $\hat{n}_{\text{orbit}}$, and the first LSS collapse axis (i.e. the perpendicular to the LSS sheet), $\hat{e}_{\text{LSS}}$.

Shao et al. 2019). The alignment of $\hat{n}_{\text{orbit}}$ with the halo minor axis, $\hat{e}_{3;\,\text{halo}}$, is shown in the right-hand panel of Fig. 3. We find that, on average, $\hat{n}_{\text{orbit}}$ is better aligned with $\hat{e}_{3;\,\text{halo}}$ than the satellites' minor axis. This is true for both the full population of MW mass haloes, and even more so for the *MW-like-orbit* systems, which have a median angle between $\hat{n}_{\text{orbit}}$ and $\hat{e}_{3;\,\text{halo}}$ of only $17.3°$.

The very strong alignment between the normal to the common orbital plane of satellites and the halo minor axis for *MW-like-orbit* systems means that we can predict the orientation of the Galactic DM halo with rather small uncertainty. The most likely orientation of the MW halo, $\hat{e}_{3;\,\text{halo MW}}$, corresponds to $(l, b) = (182°, -2°)$ and the 50, 75, and 90 percentile confidence intervals correspond to angles of $17.3°$, $26.9°$, and $36.6°$, respectively. This prediction is shown in Fig. 1 by the red cross symbol for the most likely orientation of the halo minor axis, and by the two shaded regions for the 50 and 75 percentile confidence intervals.

The MW has a close neighbour, M31, which is currently located ~ 800 kpc away and is thought to be on first approach (van der Marel et al. 2012). The large distance between the two galaxies, ~ 4 times the MW halo radius, R_{200} (Cautun et al. 2020), and the fact that M31 is on first approach make it very unlikely that the MW halo shape has been affected directly by the presence of M31. However, as we will discuss in Section 3.4, since both the MW and M31 form in the same large-scale tidal field, we expect that the MW has a weak tendency to align with this tidal field and, in turn, to align with the MW–M31 direction, which is, to a much larger degree, determined by the large-scale tidal field (van Leeuwen, in preparation). We note that the alignment between halo shapes and the tidal field is taken into account in Fig. 3 and, in fact, it is one of the key processes responsible for the results shown in the figure.

The alignment of the normal to the common orbital plane of satellites with the halo minor axis is better than the galaxy–halo minor axis alignment, which has a median angle of $33°$ (e.g. Shao et al. 2016), and thus provides a more robust way to infer the DM halo orientation. This is especially the case for systems in which many satellites have coplanar orbits, such as our Galaxy.
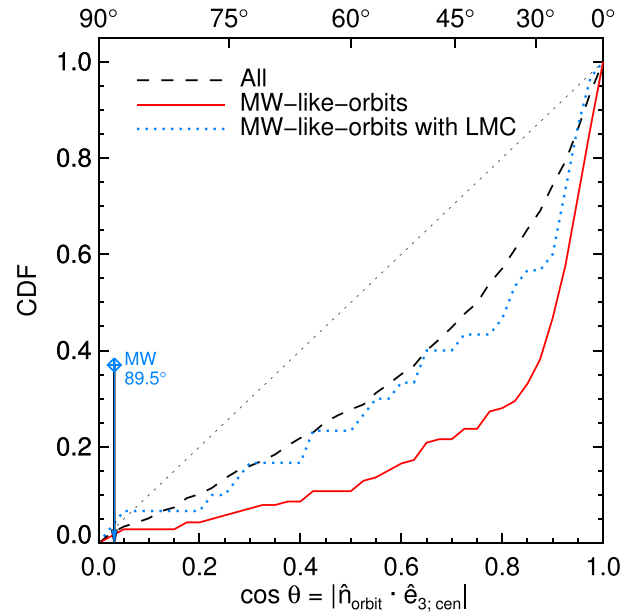

Figure 4. The CDF of the alignment angle, $\cos\theta$, between the normal, $\hat{n}_{\text{orbit}}$, to the preferential orbital plane and the minor axis, $\hat{e}_{\text{cen}}$, of the stellar disc. The vertical arrow at $\cos\theta \approx 0$ indicates the measured value for our galaxy.

We note that the MW is an extreme object in the *MW-like-orbits* sample, which has been selected to have opening angles $\alpha_8 < 35°$, while the MW has $\alpha_8^{MW} = 22°$. We find that satellite systems with α_8 values similar to that of the MW (such systems are very rare, with only 10 out of 1080 having $\alpha_8 < 25°$) show an even tighter alignment between the common orbital plane and the DM halo orientation and thus potential future studies that have access to larger cosmological simulations could constrain the Galactic halo orientation even better. Here, we do not quote any numbers because the small sample size precludes us obtaining statistically robust results.

3.3 The alignment of satellite systems with their central galaxies

In Fig. 4, we study how the satellite systems are oriented relative to the disc of the central galaxy. This is motivated by our own Galaxy, where the common orbital plane of satellites is perpendicular to the MW stellar disc (see Fig. 1 where the MW disc corresponds to $b = 0°$). We calculate the minor axis of central galaxies using equation (1), where the sum is over all the stellar particles within a radius of 10 kpc from the centre of a galaxy. The minor axis can be robustly determined since the majority (99 per cent) of galaxies have minor to major axial ratio, c/a, less than 0.9. We show results for our full sample of MW mass galaxies, which consists of both disc and spheroid morphologies.

We find that, on average, $\hat{n}_{\text{orbit}}$ is preferentially aligned with the minor axis of the stellar distribution, $\hat{e}_{3;\,\text{cen}}$, with a median angle of $41.3°$. The alignment is even stronger for the *MW-like-orbits* subsample; however, the presence of an LMC reduces this alignment, as shown by the blue dotted line. Due to the small number of *MW-like-orbit* systems with an LMC mass satellite (there are 30 such objects), we cannot exclude that the differences between the red solid and blue dotted lines in Fig. 4 are due to stochastic effects; a KS test finds that the two curves are consistent at the 1.8σ level.

Fig. 4 illustrates that the satellite orbits are preferentially in the plane of the central galaxy disc (see e.g. Lovell et al. 2011;

Cautun et al. [2015a](#)) and that this alignment is even stronger for *MW-like-orbit* systems, in which the majority of satellites have coplanar orbits. As we have seen from Fig. [3](#), the *MW-like-orbit* systems are also the ones most strongly aligned with the halo minor axis. When taken together, it suggests that satellites with coplanar orbits are preferentially found in systems in which the minor axes of the stellar disc and the DM halo are well aligned. Such configurations correspond to systems in which the directions of anisotropic infall have been roughly constant over time, since, on average, the orientation of the stellar component is determined by the early filaments along which gas was accreted while the orientation of the DM halo is determined by late time filaments (e.g. see Vera-Ciro et al. [2011](#); Wang et al. [2011](#)).

The same argument also explains why we would expect systems with a massive satellite to have a higher degree of misalignment between their satellite distribution and their central galaxies, as seen when comparing the *MW-like-orbits* and *MW-like-orbits* with LMC samples in Fig. [4](#). A more massive satellite indicates a later assembly of the host halo (Amorisco [2017](#)) and thus a larger time span between when most stars were formed and when the satellites were accreted. This increases the chance that the early filaments along which gas was accreted are misaligned with the late time filaments along which satellites fall into the system.

The MW, with a satellite system which is perpendicular to the stellar disc, is an outlier when compared to the typical EAGLE system (see Fig. [4](#)). None the less, we do find EAGLE examples that have the same satellites–stellar disc geometry as the MW. To assess how atypical the MW satellite system is, we define perpendicular configurations as the ones for which $\cos\theta \leq 0.2$. There are 5 out of 139 ($\sim$4 per cent) such perpendicular configurations in the *MW-like-orbits* sample and 3 out of 30 ($\sim$10 per cent) in the *MW-like-orbits* with LMC mass satellite sample. Thus, the MW satellites–stellar disc configuration is rather unusual, but less so when accounting for the fact that the MW has a very bright satellite. In Section 4, we study in more detail the five *MW-like-orbit* systems that most closely resemble our Galactic satellite distribution and investigate their formation history in detail.

3.4 The alignment of satellite systems with the surrounding large-scale structure

As discussed previously, anisotropic infall is one of the driving factors behind the formation of flattened and rotating satellite distributions (e.g. Libeskind et al. [2005](#), [2011](#), [2014](#); Deason et al. [2011](#); Lovell et al. [2011](#); Shao et al. [2018a](#)). The same process, anisotropic accretion of DM and gas, is responsible, at least partially, for the alignments between the DM, gas, and satellite distribution studied in the previous subsections, and it further implies that these components are preferentially aligned with the LSS in which they are embedded (e.g. Tempel et al. [2015](#); Velliscig et al. [2015b](#); Welker et al. [2015](#); Shao et al. [2016](#); Ganeshaiah Veena et al. [2018](#), [2019](#)). This motivates us to study the alignment between satellite systems and the surrounding LSS, and compare it with Galactic observations.

We determine the orientation of the LSS using the NEXUS+ algorithm (Cautun, van de Weygaert & Jones [2013](#); Cautun et al. [2014a](#); for a comparison with other cosmic web finders, see Libeskind et al. [2018](#)). This is a multiscale method that naturally determines the scale at which the mass distribution is most anisotropic and that automatically determines cosmic web environments, such as nodes, filaments, and walls. NEXUS+ takes as input the total matter density field smoothed on a range of scales using a Gaussian filter. For each smoothing scale, the method calculates the Hessian
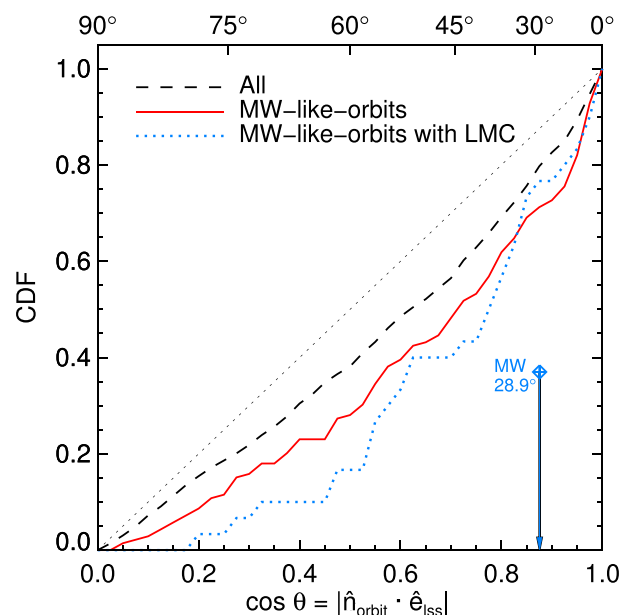

Figure 5. The CDF of the alignment angle, $\cos\theta$, $=$ between the common orbital pole of satellites and, the normal, $\hat{e}_{\mathrm{lss}}$, to the large-scale sheet in which the system is embedded. We show results for three samples: the full population of MW mass systems (dashed black), the *MW-like-orbit* systems (solid red), and the *MW-like-orbit* systems that also have an LMC mass satellite (dotted blue). The arrow indicates the measurement for our galaxy, which we obtained using the LSS directions provided by Libeskind et al. ([2015](#)).

matrix of the smoothed density field and, using its eigenvalues, determines the degree of anisotropy of the mass distribution. At each location, NEXUS+ selects the smoothing scale with the largest degree of anisotropy and the eigenvectors of the Hessian matrix calculated for that smoothing scale are then used to define the LSS directions. Here, we study the alignment relative to the first direction of LSS collapse, which we denote with $\hat{e}_{\mathrm{LSS}}$. This direction is given by the eigenvector corresponding to the largest eigenvalue and determines the normal to the LSS sheet in which a system is embedded.

Fig. [5](#) shows the alignment between the satellite distribution, characterized in terms of $\hat{n}_{\mathrm{orbit}}$, and the LSS direction, $\hat{e}_{\mathrm{LSS}}$. We find a weak alignment between the two orientations with a misalignment angle of $51.6°$ (see Table [1](#)). It illustrates that the satellites orbit preferentially within the plane defined by the LSS sheet surrounding each system. The *MW-like-orbit* systems show an even better alignment with the LSS than the full population. Furthermore, the subsample with LMC mass satellites shows a hint of an even stronger alignment, but that sample is too small to arrive at statistically robust conclusions. The weak present-day alignment between the satellite distribution and the LSS orientation is to be expected. This alignment is largest when calculated at the time of infall of the satellites (Libeskind et al. [2014](#); Shao et al. [2018a](#)), and is weakened by the subsequent evolution and rearrangement of the cosmic web around each halo (e.g. Vera-Ciro et al. [2011](#); Cautun et al. [2014a](#)).

To compare with the MW, we have calculated the angle between the MW common orbital plane and the normal to the LSS as found by Libeskind et al. ([2015](#)). The latter was calculated using the reconstructed velocity shear tensor in the Local Universe. We find that the MW satellite distribution has a $29°$ misalignment angle with respect to the local LSS sheet, in qualitative agreement with our theoretical predictions. van Leeuwen (in preparation) has studied

Table 2. Selected properties of the five systems in the EAGLE simulation that have similar satellite distributions to the MW's. The systems were chosen to have 8 of the 11 brightest satellites orbiting within a cone of opening angle, $\alpha_8 < 35°$, and in a common orbital plane close to perpendicular ($\theta > 78°$) to the stellar disc of the central galaxy. The columns are as follows: (1) system label, (2) halo mass, (3) halo radius, (4) stellar mass, (5) the angle, $\theta_{orbit–halo}$, between the common satellite orbital plane and the halo minor axis, (6) the angle, $\theta_{orbit–cen}$, between the common satellite orbital plane and the central galaxy minor axis, (7) the angle, $\theta_{halo–cen}$, between the minor axes of the DM halo and central galaxy, and (8) the stellar mass of the LMC analogue if the system has one.

Label	M_{200} $(10^{10}\ M_\odot)$	R_{200} (kpc)	$M_\star$ $(10^{10}\ M_\odot)$	$\theta_{orbit–halo}$ (deg)	$\theta_{orbit–cen}$ (deg)	$\theta_{halo–cen}$ (deg)	$M_{\star\,LMC}$ $(10^9\ M_\odot)$
MW1	125.2	227.2	2.57	2.0	72.9	70.9	1.8
MW2	97.8	209.2	3.38	5.3	80.4	78.9	–
MW3	87.3	201.4	1.82	27.9	88.9	89.0	4.1
MW4	76.0	192.4	0.98	9.8	88.3	82.5	2.7
MW5	37.4	151.9	0.64	31.3	88.5	67.0	–

the cosmic web around Local Group-like objects to find that $\hat{e}_{LSS}$ is typically determined by the mass distribution on 2 Mpc scales and that $\hat{e}_{LSS}$ shows a strong tendency to be perpendicular on the direction connecting the two Local Group members.

4 THE STRUCTURE AND FORMATION HISTORY OF THE GALACTIC DM HALO

As we discussed in the introduction, the MW classical satellites have several properties that make them atypical of galactic satellite systems in a ΛCDM universe. Previous studies have invoked such features and potential tensions with the standard cosmological model (e.g. Ibata et al. 2014; Pawlowski et al. 2014; Cautun et al. 2015b). However, while the Galactic disc of satellites is rare, it is not rare enough to pose a serious challenge to the ΛCDM model (for details see Cautun et al. 2015b, and in particular their discussion of the look-elsewhere effect). Here, we take a different approach. We assume that ΛCDM is the correct cosmological model and pose the question: what do the atypical features of the MW satellite distribution reveal about the structure and formation history of our DM halo?

We identify MW analogues in the EAGLE simulation that share the two characteristics of the satellite distribution that stand out the most: (i) that 8 of the 11 classical satellites have nearly coplanar orbits, and (ii) that the common orbital plane of those satellites is perpendicular to the stellar disc. These criteria correspond to selecting from the *MW-like-orbits* subset the systems for which the satellite distribution is nearly perpendicular to the central disc (see Section 4), which we define as having a misalignment angle, $\theta > 78°$ (i.e. $\cos\theta < 0.2$). We find five such systems, which we label MW1 to MW5, and whose properties are summarized in Table 2.

4.1 The structure of the DM halo

We start by studying the shape of the DM halo of our MW analogues as a function of the distance from the halo centre, as illustrated in Fig. 6. For each radial bin, we calculate the shape of the mass distribution within that radius. The inner regions of the halo are only slightly flattened, with $b/a \sim 0.95$ and $c/a \sim 0.85$, and the axial ratios show very little variation with radius; we can therefore make robust predictions for the shape of the inner DM halo. We note that the inner haloes in simulations that include baryons are typically rounder than in DM-only simulations (Bailin et al. 2005; Velliscig et al. 2015a; Chua et al. 2019; Prada et al. 2019), with the dominant effect being the potential of the baryons, which is very important for $r/R_{200} \le 0.2$. At larger distances, the haloes become systematically
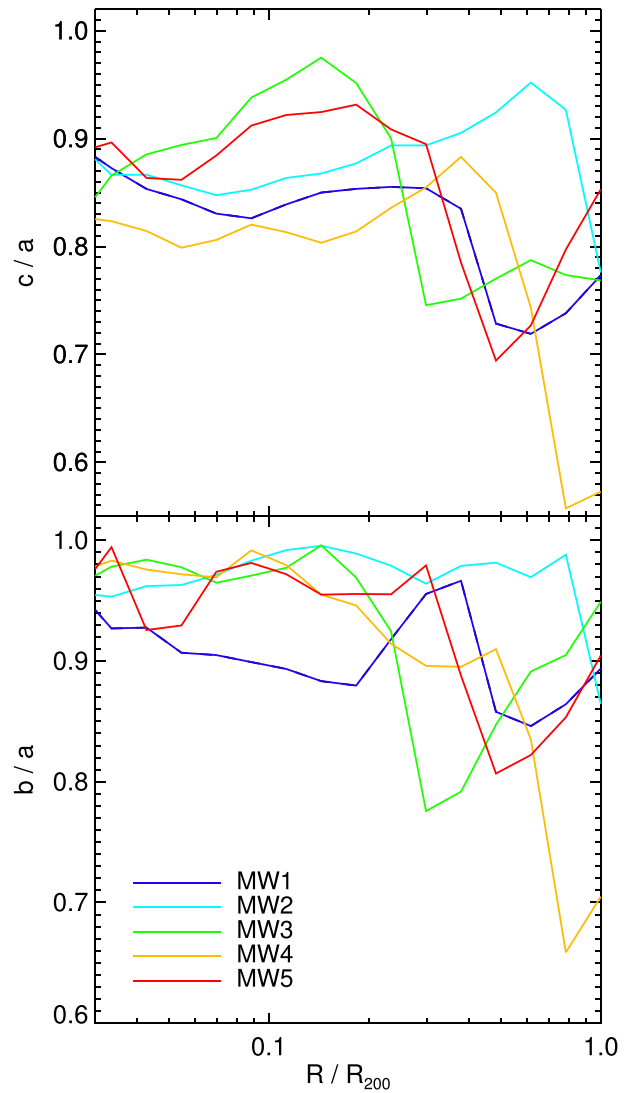

Figure 6. The $z = 0$ axial ratios, c/a (top panel) and b/a (bottom panel), for the five MW analogues that have satellite distributions similar to the MW system. The axial ratios are shown as a function of the radial distance from the halo centre, normalized by the halo radius, R_{200}. Each point corresponds to the shape of the DM particle distribution enclosed in a sphere of the given radius.
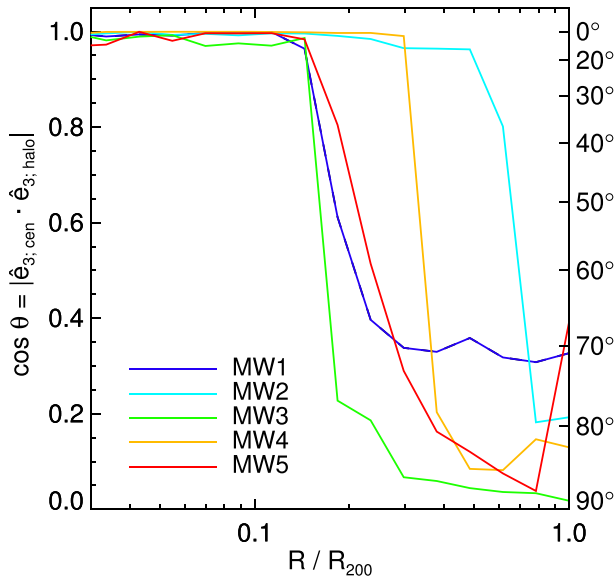
Figure 7. The alignment angle, $\cos\theta$, between the minor axes of the central stellar disc and of the DM halo. The halo shape is calculated as a function of radial distance. Each curve shows one of our five MW analogues. The twist in the halo orientation, which is visible as a rapid change in the alignment angle, reflects the fact that the outer halo is aligned with the satellite distribution, which is perpendicular on the central disc.

more flattened and, at the same time, show greater halo-to-halo variation.

We next examine how the orientation of the DM halo changes as a function of radial distance. This is illustrated in Fig. 7, which shows the alignment between the minor axes of the central galaxy and the DM halo. The inner halo is very well aligned with the stellar distribution, as seen in other galaxy formation simulations (see also Bailin et al. 2005; Tenneti et al. 2014; Velliscig et al. 2015a; Shao et al. 2016). But, at farther distances, we see a very rapid shift in the DM halo orientation, which changes by more than 70° over a very narrow radial range. We refer to this feature as the 'twist' of the DM halo. The exact radius where the twist takes place varies from system to system, but the existence of such a twist is a robust feature across all our MW analogues. At even larger distances, the halo orientation remains fairly stable and nearly perpendicular to DM distribution in the inner region.

We have checked that the halo 'twist' seen in Fig. 7 does not depend on the definition used to calculate the halo shape. A similar twist is seen if instead we were to use the reduced mass tensor (Frenk et al. 1988; Dubinski & Carlberg 1991), with the only difference being that the twist is not as sharp. This difference is due to the reduced tensor giving equal weight to all DM particles, so we need to include more particles (i.e. go to larger radii) outside the twist radius to see it. Similarly, in the three cases that have an LMC mass satellite, the twist is not determined by the LMC's DM particles. We checked this by removing all particles associated with the LMC mass satellite before infall into their MW mass host. The orientation of the halo and the twist radius hardly change when removing the DM particles associated with the LMC mass satellite.

In Fig. 8, we present a more intuitive way of visualizing the orientation of the DM halo for our three MW analogues (MW1, MW3, and MW4) that have an LMC mass satellite. The left-hand panels show the minor axis of the halo calculated at various radial distances. The sky coordinates are fixed according to the stellar

distribution of each central galaxy, with the plane of the disc corresponding to $b = 0°$. The sky projection clearly shows the twist of the DM halo: the minor axis of the halo, which is found at $b \sim 90°$ in the inner regions, undergoes a rapid change to $b \sim 0°$ at large radial distances. The panels also illustrate that the minor axis orientation generally varies by $\sim 10°$ or less between neighbouring bins, a signature of a smooth change in the different directions along which the halo assembled (Vera-Ciro et al. 2011). However, the halo 'twist' represents a dramatic change in orientation, with the minor axis varying by $\sim 70°$ from one radial bin to the next. This suggests that, to a good approximation, these DM haloes can be modelled as an inner component with minor axis at $b = 90°$ and an outer component with minor axis at $b \sim 0°$.

The right-hand panels of Fig. 8 illustrate both the shape and orientation in projection of the DM halo for the MW1, MW3, and MW4 systems. To highlight its relation to the stellar distribution, we select a Cartesian coordinate system in which the central galaxy is seen edge-on along the x-axis and the rotating plane of satellites is also found roughly edge-on but along the y-axis. Such geometries are possible for our sample of MW analogues since the rotating plane of satellites is perpendicular to the central disc. In each panel, the stellar distribution is shown by the background colours, with the LMC mass analogue being clearly visible as a massive blob. The halo shape and orientation are represented by ellipses, with each ellipse corresponding to the DM distribution in a sphere centred on the central galaxy. The axes of each ellipse are given by the major and minor axes of the 3D DM distribution, and the ellipse is orientated to make the same angle with the x-axis (i.e. the central stellar disc) as the 3D angle between the halo minor axis and the stellar disc. The figure provides a compelling illustration of the complex geometry that characterizes our MW analogues.

The ubiquity of a 'twist' in all our MW analogues suggests that such a feature ought to be present in our Galactic DM halo too. Unfortunately, the satellite distribution cannot constrain the exact radius where the twist would happen, which for our sample varies from 30 kpc for MW3 to 150 kpc for MW2. Evidence for a twist in the Galactic halo has been claimed before when modelling the orbit of the Sagittarius stream (see the interpretation of the Law & Majewski 2010 MW model by Vera-Ciro & Helmi 2013), but the validity of this claim has been hotly debated, especially because the massive DM halo in which the LMC resides could introduce systematic effects (see e.g. Vera-Ciro & Helmi 2013; Gómez et al. 2015). If we take the results of the Law & Majewski Galactic model at face value, then the Galactic halo twist must be inside the orbit traced by Sagittarius, potentially as close as a few tens of kiloparsecs from the Galactic Centre.

4.2 The formation of a twisted halo

We start by studying if the halo twist is a long-lived feature. We would expect this to be the case since the presence of the twist was inferred from the orbits of the classical satellites, which have an orbital period of a few Gyr. Indeed, this is the case for all our five MW analogues: the halo twist formed ~ 10 Gyr ago and, since then, has shown little change. We highlight this in Fig. 9, where, for the MW3 analogue, we plot halo orientation as a function of distance from the centre at various lookback times. We find that the twist started forming 10 Gyr ago in the matter distribution just outside the halo radius (see dotted red line in the figure). As the MW3 halo accreted that material, the twist radius shifted inwards to ~ 50 kpc and remained at that position until 4 Gyr ago. That is when the MW3 halo experiences the first pericentre passage of an LMC mass satellite; this shifted the twist
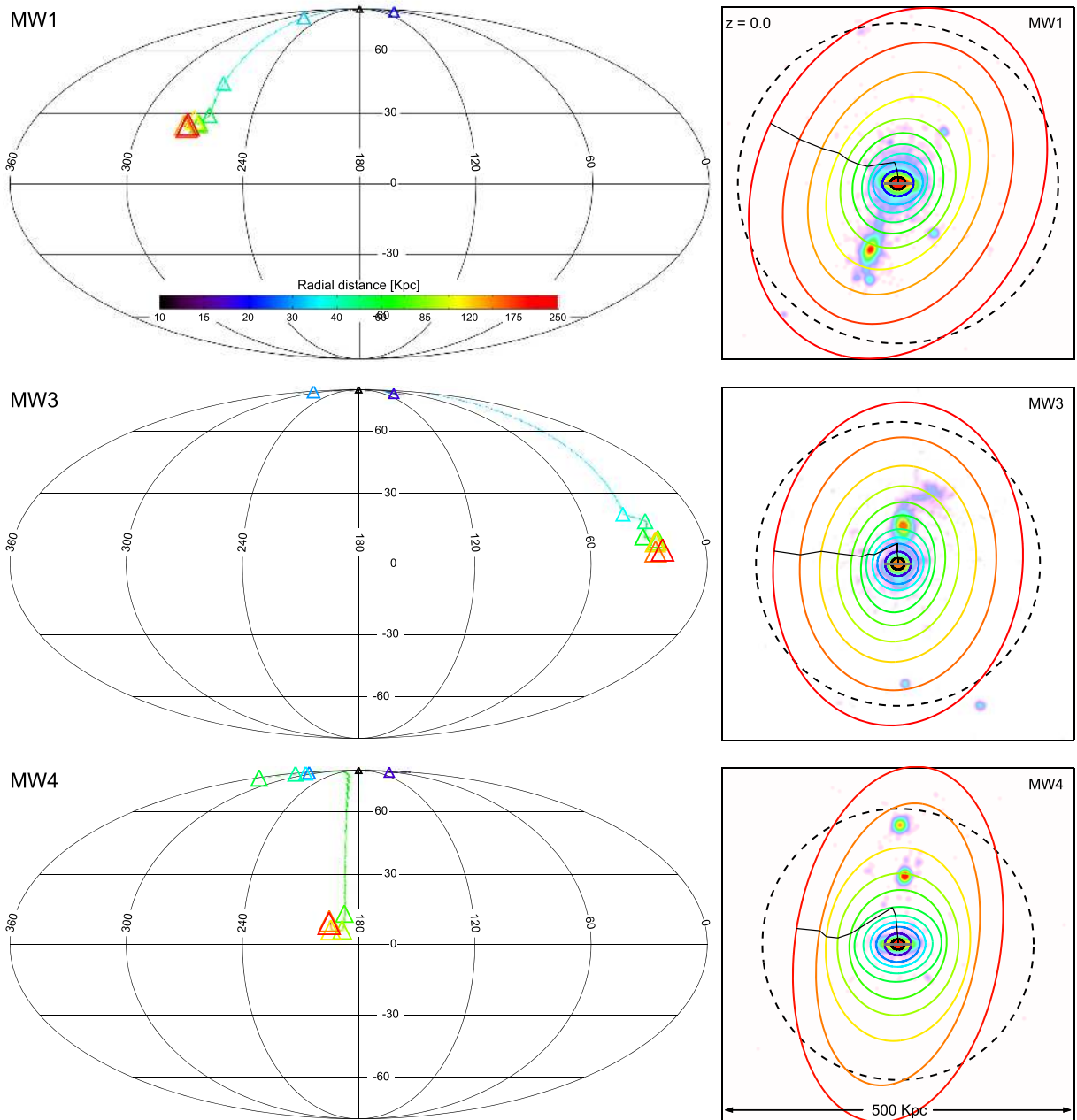
Figure 8. Left-hand panel: Aitoff projection showing the orientation of the minor axis (triangles) of the host DM halo of the three MW analogues that have an LMC mass satellite (MW1, MW3, and MW4). We measure the halo shape within spherical regions with radii between 10 kpc and R_{200} (this is different for each host, see Table 2); the colours indicate the radii as shown in the legend. The coordinate system is given by the central galaxy stellar disc, with the disc being located in the $b = 0°$ plane. Right-hand panel: The shape and orientation of the DM haloes at different radii. As for the left-hand panel, the colours indicate the radius. The background image shows the distribution of stars with the central galaxy seen edge-on along the x-axis and the rotating satellite distribution seen edge-on along the y-axis. The main axes of each ellipse are given by the major and the minor axis of the DM distribution within each 3D radius. Each ellipse is oriented such that it makes the same angle with the x-axis (i.e. the disc of the central galaxy) as the 3D angle between the minor axis of the halo and the stellar disc. For clarity, the position of the minor axis is highlighted by the solid black line that connects the various ellipses. The black dashed line shows the halo radius, R_{200}.

inwards to a distance of 30 kpc from the centre, where it has remained until the present day. Three of our five MW analogues experience an inward shift of the halo twist radius: two of the three systems with an LMC mass satellite and one of the two systems without an LMC analogue.

Fig. 9 also highlights that after formation the twist radius is rather sharp, with the exception of the transient stage when the twist moves

inwards. Moreover, the twist formed prior to the infall of massive satellites that survive to present day. For example, MW3 has a massive LMC analogue satellite that brought in 20 per cent of the $z = 0$ total mass of the system. In this case, the twist was fully formed already 8 Gyr ago, when the LMC analogue was over 300 kpc from the host halo centre. As we shall discuss next, the twist is associated with a change in the orientation of the dominant cosmic web filament
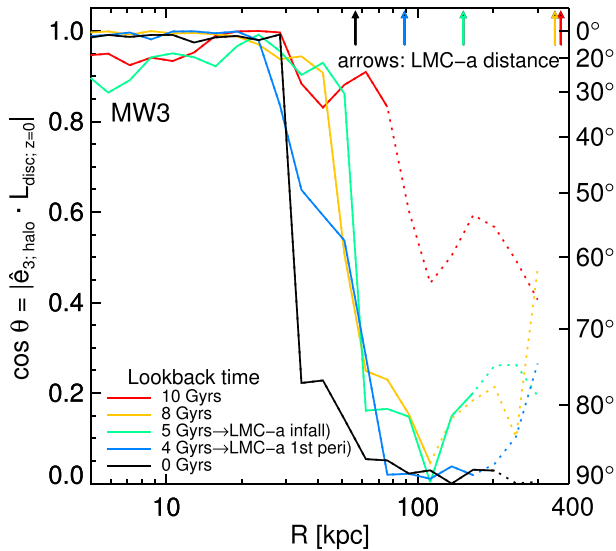
Figure 9. Time evolution of the alignment angle between the central galaxy's angular momentum and the minor axis of the DM halo for the MW analogue MW3. As in Fig. 7, the halo shape is calculated as a function of distance from the centre, which is shown on the *x*-axis. The various lines show the system at lookback times of 10, 8, 5, 4, and 0 Gyr. The shape of the matter distribution for the large R bins was calculated using also DM particles outside the halo radius and, to distinguish them, those results are shown by a dotted line. The vertical arrows indicate the radial distance of the LMC analogue satellite.

feeding the system, which brings in a large amount of mass into the growing halo.

We now investigate the effects that produce a twist in the DM haloes in all our MW analogues. We focus on answering two questions: (i) is the twist produced because the spin of the stellar disc flipped at some point as a result of either a merger with or a flyby by other galaxies (e.g. Bett & Frenk 2012, 2016; Dubois et al. 2014; Earp et al. 2017)? or (ii) is the twist due to a variation in the direction of the (anisotropic) infall of satellites?

To answer these questions, we follow the variation in time of the orientation of the central galaxies and their DM haloes in each of our MW analogues. This is shown in Fig. 10 where we plot the orientation relative to that at the present day. We find that the orientation of the central discs has been relatively stable in the past 5 Gyr and potentially even longer for some systems, such as MW2 and MW4. During the last several gigayears, the discs experience only minor changes in orientation (see also Earp et al. 2019), typically ≲20°; these cannot explain the ~90° misalignment between the stellar and DM components in our MW analogues. At early times, the orientation of the stellar disc can vary more rapidly (see e.g. MW1 in the top panel of Fig. 10) but this is typically the period when the stellar mass was only a small fraction of today's value (see Fig. A1 in the Appendix).

In the bottom panel of Fig. 10, we study the changes in the orientation of the DM halo. We see rather large variations even at late times (e.g. MW5): the orientation of the halo is much less stable in time than that of the stellar disc. The orientation of the halo is affected by recently accreted material, which, being at large distances from the halo centre, makes a large contribution to the mass tensor. The distribution of recently accreted material is determined by the geometry of the cosmic web surrounding the system and, thus, the variation in halo orientation is a manifestation of variations in the LSS within which it is embedded. We have confirmed this
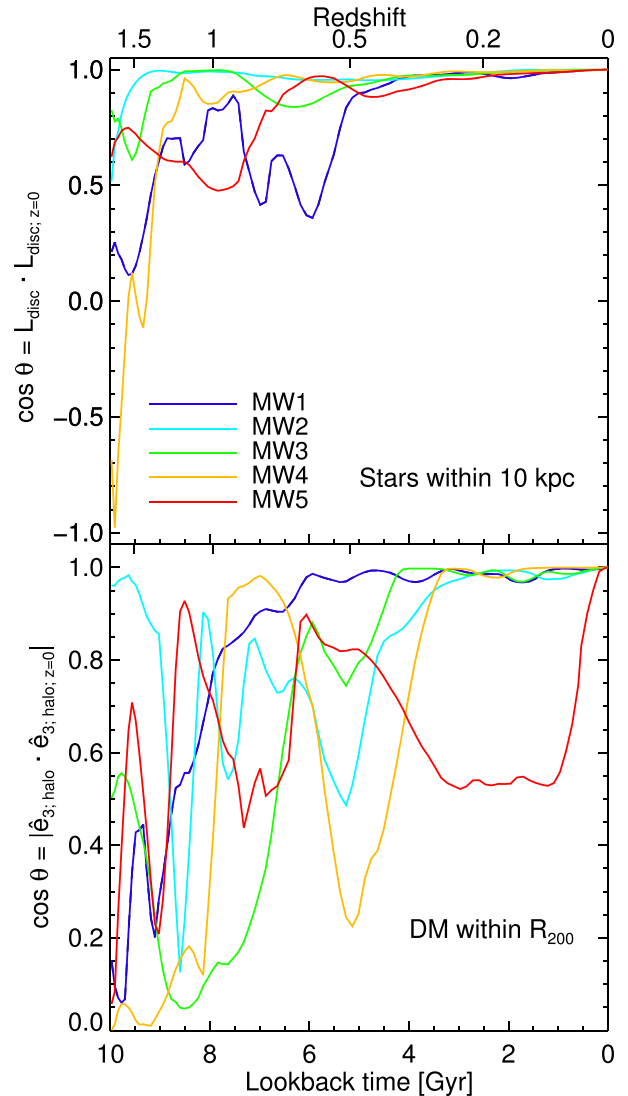

Figure 10. Top panel: The orientation of the central galaxy's angular momentum at different stages of the formation history. The orientation is relative to the direction of angular momentum at $z = 0$. Bottom panel: The same but for the minor axis of the whole DM halo.

point visually by viewing movies of the evolution of these systems. They show that the filaments feeding the halo can vary in time, especially between early ($z > 1$) and late ($z < 0.5$) epochs, and that the variation is due to a mismatch between the small-scale cosmic web which feeds the early growth of the halo and the slightly larger scale web that is important for the late halo growth. The evolution of one such system, MW3, is illustrated in Fig. 11, which shows the DM distribution surrounding the halo from $z = 2.5$ up to present day. Note that, in general, the small- and large-scale webs are well aligned (Aragón Calvo 2007; Rieder et al. 2013). The small and rather special sample of systems we are considering here are not representative of the average ΛCDM halo.

We also checked that the sudden change in halo orientation is not due to the accretion of the LMC mass analogues found in the MW1, MW3, and MW4 systems. In fact, the DM halo changes orientation before the LMC analogue falls in (see Fig. B1 in the Appendix for the orbits of the LMC analogues). This is to be expected since the most massive satellites are accreted along the most prominent filament
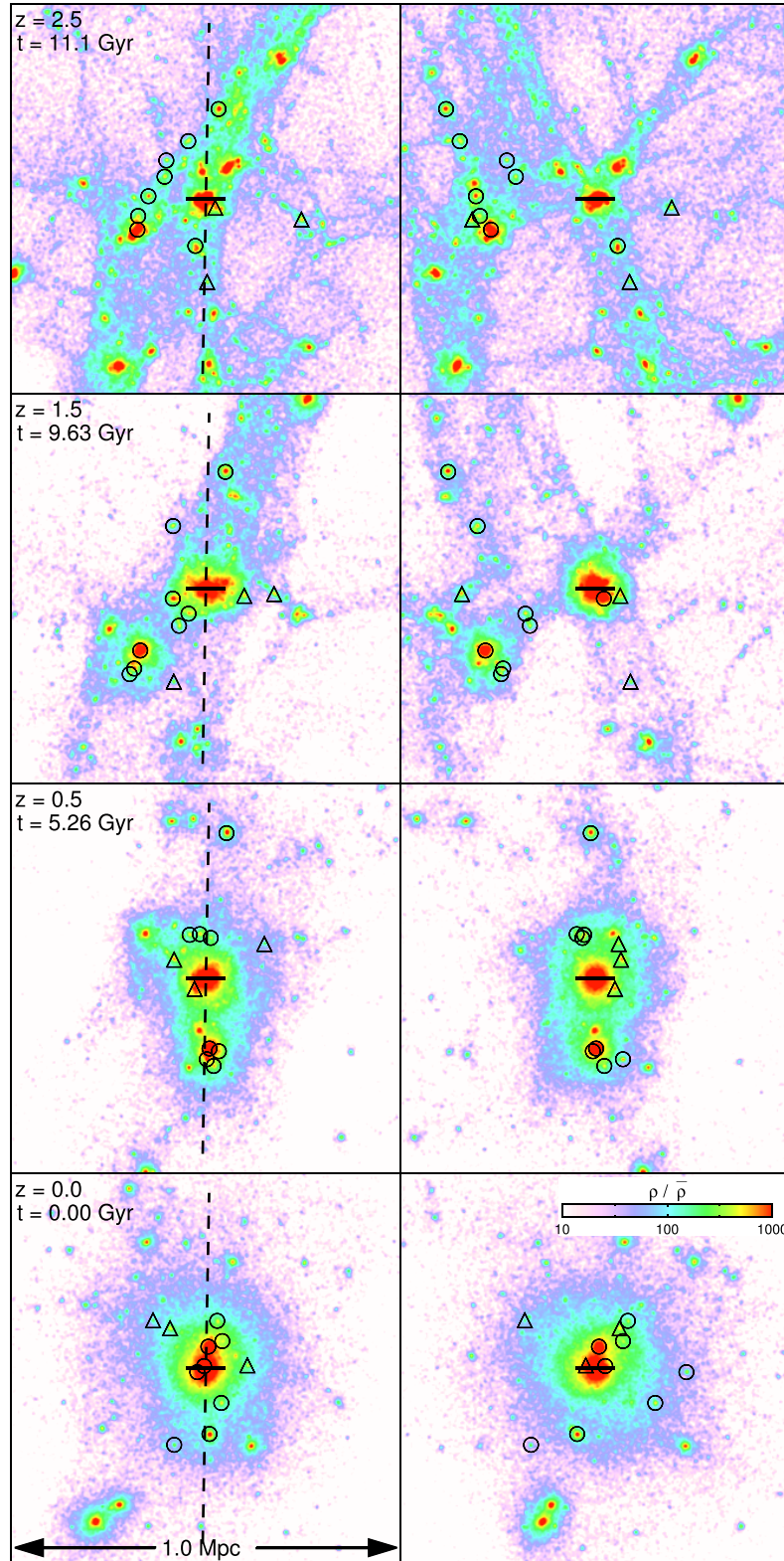
Figure 11. The evolution of the DM distribution within 0.5 physical Mpc around one of our MW analogues, MW3. The colours show the projected DM density, with red colours corresponding to high-density regions and white corresponding to low-density regions (see colour bar in the bottom right panel). The rows show the system at redshifts: 2.5, 1.5, 0.5, and 0.0, respectively. The left-hand column corresponds to the coordinate system in which the disc of the central galaxy at $z = 0$ is seen edge-on along the x-axis (see horizontal black solid line) and the rotating plane of satellites at $z = 0$ is seen also edge-on but along the y-axis (vertical black dashed line). The right-hand column shows the system after a $90°$ rotation, with the central disc still seen edge-on along the x-axis but with the rotating plane of satellites seen face-on. The satellites and their progenitors are shown as open circles (for the 8 out of the 11 brightest satellites with coplanar orbits at $z = 0$) and open triangles (for the remaining 3 satellites).

(Shao et al. 2018a) and that is already in place before the infall of the LMC analogue. It is this prominent filament, along which the LMC analogue falls in, that determines the orientation of the host halo.

5 CONCLUSIONS

We have analysed analogues of the MW in the EAGLE cosmological hydrodynamics simulation of galaxy formation in order to learn about the likely structure, shape, and orientation of the MW's DM halo. Our sample of MW analogues consists of EAGLE haloes of mass $M_{200} \sim 10^{12}$ M$_\odot$ whose brightest 11 satellites have similar spatial and kinematical properties to the classical satellites of our Galaxy. In particular, we defined the subset of '*MW-like-orbit*' systems as those in which the majority of the satellites orbit in a single plane. This selection was motivated by the observation of Shao et al. (2019, see also Pawlowski et al. 2013) that 8 out of the 11 classical MW satellites have orbital poles that lie within a very narrow, $\alpha_8^{\mathrm{MW}} = 22°$, opening angle. To obtain a reasonably sized sample of counterparts in the relatively small volume of the EAGLE simulation [(100Mpc)^3)], we relaxed the criterion slightly, requiring that 8 of the brightest 11 satellites should have orbital poles within an $\alpha_8 = 35°$ opening angle.

From our subsample of *MW-like-orbit* DM haloes, we conclude:

(i) Haloes that, like that of the MW, host coplanar satellite orbits tend to be more flattened (lower c/a axial ratio) than the full population of haloes of similar mass. The *MW-like-orbit* systems also have b/a ratios closer to unity than the full sample (see Fig. 2).

(ii) The normal to the common orbital plane of satellites is well aligned with the minor axis of the DM host halo. The alignment is even stronger for the *MW-like-orbit* subsample (see Fig. 3).

(iii) From these results, we predict that the minor axis of the actual MW DM halo should be pointing along the direction $(l, b) = (182°, -2°)$, with the 50, 75, and 90 percentile confidence intervals corresponding to angular uncertainties of $17.3°$, $26.9°$, and $36.6°$, respectively (see Fig. 1).

(iv) The common orbital plane of satellites in the simulations is preferentially aligned with the central stellar disc, but this alignment is not as strong as that with the DM halo (see Fig. 4).

(v) The presence of an LMC mass satellite does not affect the satellite orbital plane–DM halo alignment, but it weakens the satellite orbital plane–central disc alignment.

(vi) The planes of satellites have only a weak alignment with the present-day LSS environment in which they are embedded (see Fig. 5).

The MW satellite distribution has another unusual feature: the common orbital plane (and the associated plane of satellites) is almost perpendicular to the stellar disc. Such configurations are rare in the EAGLE simulation, where most satellites orbit in the plane of the central galaxy. To understand the implications of this strange perpendicular arrangement, we selected those *MW-like-orbit* systems in which the majority of bright satellites orbit in the plane perpendicular to the stellar disc. Only five such examples are to be found in EAGLE, corresponding to ~4 per cent of the *MW-like-orbit* sample. Three out of the five have an LMC mass satellite indicating that the presence of a massive satellite makes a perpendicular configuration between the orbits of satellites and the central disc more likely.

From this subset of five MW analogues, which represent the closest match in EAGLE to the spatial and kinematical distribution of classical satellites in the MW, we find:

(i) In the inner ~30 kpc, the haloes of the MW analogues have axial ratios, $b/a = 0.85$ and $c/a = 0.95$, with little halo-to-halo variation. The outer parts of the halo are more flattened than the inner parts and show larger halo-to-halo variation (see Fig. 6).

(ii) The DM halo of each MW analogue is 'twisted' such that the orientation of the outer halo is perpendicular to that of the inner halo. Since the main plane of the inner halo is aligned with the central disc, the outer halo is nearly perpendicular to the stellar disc. The location of the twist varies amongst haloes, but always occurs suddenly, in a very narrow radial range (see Fig. 7).

(iii) In all our MW analogues, the twist is due to a shift in the direction of (anisotropic) accretion between early and late times, which is reflected in the different orientations of the inner and outer DM halo. The central disc is quite stable once most of the stars have formed, at redshift, $z \lesssim 0.5$ (or ~5 Gyr lookback time).

Cosmological hydrodynamical simulations predict that the central galaxy and the outer halo can be misaligned, with a median angle of $33°$ (e.g. Bett et al. 2007; Tenneti et al. 2015; Velliscig et al. 2015a; Shao et al. 2016). However, only a small fraction of systems have a ~90° misalignment, which is what we predict to be the case for the MW. For example, only ~10 per cent of our MW mass sample consists of cases where the outer halo is close to perpendicular (i.e. at an angle of 80° or higher) to the stellar disc. The MW's misaligned DM halo is another feature, on top of the plane of satellite galaxies, that makes our galaxy stand out.

The 'twisted' DM halo inferred for our Galaxy by our analysis is consistent with the Galactic model proposed by Vera-Ciro & Helmi (2013) in which the inner halo is aligned with the MW disc while the outer halo is perpendicular to it. This model is based on the analysis of the orbit of the Sagittarius stream by Law & Majewski (2010) who argued that this requires the minor axis of the Galactic halo to be perpendicular to the stellar disc. Furthermore, our prediction for the orientation of the minor axis of the halo, $(l, b) = (182°, -2°)$, matches very well the orientation inferred by Law & Majewski,[2] $(l, b) = (187°, 0°)$. We note that the halo orientation inferred by Law & Majewski is still a matter of debate, largely because it ignores the gravitational influence of the LMC (Vera-Ciro & Helmi 2013; Gómez et al. 2015), which is thought to be rather massive (Peñarrubia et al. 2016; Laporte et al. 2018; Shao et al. 2018b; Cautun et al. 2019) and this could introduce systematic uncertainties. In a recent study, Erkal et al. (2019) have argued that even when including the LMC potential, the orbit of the Orphan stream prefers an oblate Galactic halo with minor axis pointing towards $(l, b) = (176.2°, -13.1°)$; this agrees very well with our own prediction for the orientation of the outer halo. Thus, our study provides independent and robust evidence that our Galactic DM halo is indeed 'twisted', a conclusion that could perhaps be tested further with *Gaia* data.

One of the limitations of our analysis is that, in order to obtain a large sample of MW-like systems, we had to relax the criteria for selecting satellite distributions with a majority of coplanar satellite orbits. Our *MW-like-orbit* sample consists of systems where eight satellites have orbital poles within opening angle, $\alpha_8 = 35°$, while for the MW the opening angle is $\alpha_8^{\mathrm{MW}} = 22°$. We find that limiting our analysis to systems with small α_8 values leads to an even tighter alignment between the normal to the common orbital plane of satellites and the halo minor axis although with increased

---

[2]We applied a 180° shift in l to the value reported by Law & Majewski to account for the fact that we measure an orientation and not a vector (i.e. both vectors **x** and $-\mathbf{x}$ correspond to the same orientation).

noise. Future simulations with much larger volumes than EAGLE will provide larger samples of systems with small enough values of α_8, potentially enabling more robust constrains on the orientation of the Galactic DM halo.

A larger sample of MW analogues would be needed to investigate whether the location of the twist can be inferred from the properties of the satellite sample itself. For example, satellites accreted early have fallen along different directions from satellites accreted later on, so contrasting the orbits of early versus late accreted satellites could constrain the lookback time at which the halo switched orientation. The earlier the switch, the further in it happens.

All our EAGLE MW analogues exhibit a twisted DM halo and, on this basis, we have argued, that this feature is a generic prediction of ΛCDM. While twisted haloes have so far only been identified in the EAGLE simulation, we expect this feature to be independent of the galaxy formation physics. The tight alignment between satellite orbits and the outer DM halo is driven by gravitational collapse and thus is largely insensitive to the details of baryonic physics. Similarly, the tight alignment between the central galaxy and the inner halo is a consequence of the DM in the inner regions conforming to the gravitational potential which is dominated by the baryonic distribution. Our simulations suggest that twisted DM haloes should be commonplace in a ΛCDM universe.

DATA AVAILABILITY

The EAGLE data are publicly available at http://icc.dur.ac.uk/Eagle/database.php. The data produced in this paper are available upon reasonable request to the corresponding author.

REFERENCES

Abadi M. G., Navarro J. F., Steinmetz M., Eke V. R., 2003, ApJ, 591, 499
Allgood B., Flores R. A., Primack J. R., Kravtsov A. V., Wechsler R. H., Faltenbacher A., Bullock J. S., 2006, MNRAS, 367, 1781
Amorisco N. C., 2017, MNRAS, 469, L48
Aragón Calvo M. A., 2007, PhD thesis. University of Groningen
Bailin J. et al., 2005, ApJ, 627, L17
Bett P. E., Frenk C. S., 2012, MNRAS, 420, 3324
Bett P. E., Frenk C. S., 2016, MNRAS, 461, 1338
Bett P., Eke V., Frenk C. S., Jenkins A., Helly J., Navarro J., 2007, MNRAS, 376, 215
Bose S., Deason A. J., Belokurov V., Frenk C. S., 2020, MNRAS, 495, 743
Bovy J., Bahmanyar A., Fritz T. K., Kallivayalil N., 2016, ApJ, 833, 31
Bowden A., Belokurov V., Evans N. W., 2015, MNRAS, 449, 1391
Bowden A., Evans N. W., Williams A. A., 2016, MNRAS, 460, 329
Bryan S. E., Kay S. T., Duffy A. R., Schaye J., Dalla Vecchia C., Booth C. M., 2013, MNRAS, 429, 3316
Buck T., Dutton A. A., Macciò A. V., 2016, MNRAS, 460, 4348
Busha M. T., Wechsler R. H., Behroozi P. S., Gerke B. F., Klypin A. A., Primack J. R., 2011, ApJ, 743, 117
Callingham T. M. et al., 2019, MNRAS, 484, 5453
Carlsten S. G., Greene J. E., Peter A. H. G., Greco J. P., Beaton R. L., 2020, ApJ, 902, 124
Cautun M., van de Weygaert R., Jones B. J. T., 2013, MNRAS, 429, 1286
Cautun M., van de Weygaert R., Jones B. J. T., Frenk C. S., 2014a, MNRAS, 441, 2923
Cautun M., Frenk C. S., van de Weygaert R., Hellwing W. A., Jones B. J. T., 2014b, MNRAS, 445, 2049
Cautun M., Wang W., Frenk C. S., Sawala T., 2015a, MNRAS, 449, 2576
Cautun M., Bose S., Frenk C. S., Guo Q., Han J., Hellwing W. A., Sawala T., Wang W., 2015b, MNRAS, 452, 3838
Cautun M., Deason A. J., Frenk C. S., McAlpine S., 2019, MNRAS, 483, 2185
Cautun M. et al., 2020, MNRAS, 494, 4291
Chua K. T. E., Pillepich A., Vogelsberger M., Hernquist L., 2019, MNRAS, 484, 476
Contigiani O., Rossi E. M., Marchetti T., 2019, MNRAS, 4025 , 487
Correa C. A., Schaye J., Clauwens B., Bower R. G., Crain R. A., Schaller M., Theuns T., Thob A. C. R., 2017, MNRAS, 472, L45
Crain R. A. et al., 2015, MNRAS, 450, 1937
Davis M., Efstathiou G., Frenk C. S., White S. D. M., 1985, ApJ, 292, 371
Deason A. J. et al., 2011, MNRAS, 415, 2607
Deason A. J., Belokurov V., Evans N. W., An J., 2012, MNRAS, 424, L44
Deason A. J., Fattahi A., Belokurov V., Evans N. W., Grand R. J. J., Marinacci F., Pakmor R., 2019, MNRAS, 485, 3514
Debattista V. P., Roškar R., Valluri M., Quinn T., Moore B., Wadsley J., 2013, MNRAS, 434, 2971
Deg N., Widrow L., 2013, MNRAS, 428, 912
Dolag K., Borgani S., Murante G., Springel V., 2009, MNRAS, 399, 497
Dubinski J., Carlberg R. G., 1991, ApJ, 378, 496
Dubois Y. et al., 2014, MNRAS, 444, 1453
Eadie G., Jurić M., 2019, ApJ, 875, 159
Earp S. W. F., Debattista V. P., Macciò A. V., Cole D. R., 2017, MNRAS, 469, 4095
Earp S. W. F., Debattista V. P., Macció A. V., Wang L., Buck T., Khachaturyants T., 2019, MNRAS, 488, 5728
Erkal D. et al., 2018, MNRAS, 481, 3148
Erkal D. et al., 2019, MNRAS, 487, 2685
Frenk C. S., White S. D. M., 2012, Ann. Phys., Lpz., 524, 507
Frenk C. S., White S. D. M., Davis M., Efstathiou G., 1988, ApJ, 327, 507
Gaia Collaboration, 2018, A&A, 616, A12
Ganeshaiah Veena P., Cautun M., van de Weygaert R., Tempel E., Jones B. J. T., Rieder S., Frenk C. S., 2018, MNRAS, 481, 414
Ganeshaiah Veena P., Cautun M., Tempel E., van de Weygaert R., Frenk C. S., 2019, MNRAS, 487, 1607
Garavito-Camargo N., Besla G., Laporte C. F. P., Johnston K. V., Gómez F. A., Watkins L. L., 2019, ApJ, 884, 51
Gnedin O. Y., Gould A., Miralda-Escudé J., Zentner A. R., 2005, ApJ, 634, 344
Gómez F. A., Besla G., Carpintero D. D., Villalobos Á., O'Shea B. W., Bell E. F., 2015, ApJ, 802, 128
Hahn O., Porciani C., Carollo C. M., Dekel A., 2007, MNRAS, 375, 489
Hayashi E., Navarro J. F., Springel V., 2007, MNRAS, 377, 50
Helmi A., 2004, ApJ, 610, L97
Ibata R. A., Ibata N. G., Lewis G. F., Martin N. F., Conn A., Elahi P., Arias V., Fernando N., 2014, ApJ, 784, L6
Jing Y. P., Suto Y., 2002, ApJ, 574, 538
Johnston K. V., Law D. R., Majewski S. R., 2005, ApJ, 619, 800
Kang X., Wang P., 2015, ApJ, 813, 6

Kroupa P., Theis C., Boily C. M., 2005, A&A, 431, 517

Kunkel W. E., Demers S., 1976, in Dickens R. J., Perry J. E., Smith F. G., King I. R., eds, Royal Greenwich Observatory Bulletins, Vol. 182, The Galaxy and the Local Group, Herstmonceaux, p. 241

Laporte C. F. P., Gómez F. A., Besla G., Johnston K. V., Garavito-Camargo N., 2018, MNRAS, 473, 1218

Law D. R., Majewski S. R., 2010, ApJ, 714, 229

Libeskind N. I., Frenk C. S., Cole S., Helly J. C., Jenkins A., Navarro J. F., Power C., 2005, MNRAS, 363, 146

Libeskind N. I., Cole S., Frenk C. S., Okamoto T., Jenkins A., 2007, MNRAS, 374, 16

Libeskind N. I., Knebe A., Hoffman Y., Gottlöber S., Yepes G., Steinmetz M., 2011, MNRAS, 411, 1525

Libeskind N. I., Knebe A., Hoffman Y., Gottlöber S., 2014, MNRAS, 443, 1274

Libeskind N. I., Hoffman Y., Tully R. B., Courtois H. M., Pomarède D., Gottlöber S., Steinmetz M., 2015, MNRAS, 452, 1052

Libeskind N. I. et al., 2018, MNRAS, 473, 1195

Lipnicky A., Chakrabarti S., 2017, MNRAS, 468, 1671

Lovell M. R., Eke V. R., Frenk C. S., Jenkins A., 2011, MNRAS, 413, 3013

Ludlow A. D. et al., 2013, MNRAS, 432, 1103

Lynden-Bell D., 1976, MNRAS, 174, 695

Lynden-Bell D., 1982, Observatory, 102, 202

Malhan K., Ibata R. A., 2019, MNRAS, 486, 2995

McAlpine S. et al., 2016, Astron. Comput., 15, 72

McConnachie A. W., 2012, AJ, 144, 4

Patel E., Besla G., Mandel K., Sohn S. T., 2018, ApJ, 857, 78

Patel E. et al., 2020, ApJ, 893, 121

Pawlowski M. S., Kroupa P., Jerjen H., 2013, MNRAS, 435, 1928

Pawlowski M. S. et al., 2014, MNRAS, 442, 2362

Peñarrubia J., Gómez F. A., Besla G., Erkal D., Ma Y.-Z., 2016, MNRAS, 456, L54

Planck Collaboration XVI, 2014, A&A, 571, A16

Posti L., Helmi A., 2019, A&A, 621, A56

Prada J., Forero-Romero J. E., Grand R. J. J., Pakmor R., Springel V., 2019, MNRAS, 490, 4877

Price-Whelan A. M., Hogg D. W., Johnston K. V., Hendel D., 2014, ApJ, 794, 4

Qu Y. et al., 2017, MNRAS, 464, 1659

Rieder S., van de Weygaert R., Cautun M., Beygu B., Portegies Zwart S., 2013, MNRAS, 435, 222

Sanders J. L., Binney J., 2013, MNRAS, 433, 1826

Schaye J. et al., 2015, MNRAS, 446, 521

Schneider M. D., Frenk C. S., Cole S., 2012, J. Cosmol. Astropart. Phys., 2012, 030

Shao S., Cautun M., Frenk C. S., Gao L., Crain R. A., Schaller M., Schaye J., Theuns T., 2016, MNRAS, 460, 3772

Shao S., Cautun M., Frenk C. S., Grand R. J. J., Gómez F. A., Marinacci F., Simpson C. M., 2018a, MNRAS, 476, 1796

Shao S., Cautun M., Deason A. J., Frenk C. S., Theuns T., 2018b, MNRAS, 479, 284

Shao S., Cautun M., Frenk C. S., 2019, MNRAS, 488, 1166

Somerville R. S., Davé R., 2015, ARA&A, 53, 51

Springel V., 2005, MNRAS, 364, 1105

Springel V., Yoshida N., White S. D. M., 2001, New Astron., 6, 79

Tempel E., Guo Q., Kipper R., Libeskind N. I., 2015, MNRAS, 450, 2727

Tenneti A., Mandelbaum R., Di Matteo T., Feng Y., Khandai N., 2014, MNRAS, 441, 470

Tenneti A., Mandelbaum R., Di Matteo T., Kiessling A., Khandai N., 2015, MNRAS, 453, 469

Trayford J. W. et al., 2015, MNRAS, 452, 2879

van der Marel R. P., Alves D. R., Hardy E., Suntzeff N. B., 2002, AJ, 124, 2639

van der Marel R. P., Fardal M., Besla G., Beaton R. L., Sohn S. T., Anderson J., Brown T., Guhathakurta P., 2012, ApJ, 753, 8

Velliscig M. et al., 2015a, MNRAS, 453, 721

Velliscig M. et al., 2015b, MNRAS, 454, 3328

Vera-Ciro C., Helmi A., 2013, ApJ, 773, L4

Vera-Ciro C. A., Sales L. V., Helmi A., Frenk C. S., Navarro J. F., Springel V., Vogelsberger M., White S. D. M., 2011, MNRAS, 416, 1377

Wang J. et al., 2011, MNRAS, 413, 1373

Wang W., Han J., Cautun M., Li Z., Ishigaki M. N., 2020, Science China Physics, Mechanics, and Astronomy, 63, 109801

Warren M. S., Quinn P. J., Salmon J. K., Zurek W. H., 1992, ApJ, 399, 405

Watkins L. L., van der Marel R. P., Sohn S. T., Evans N. W., 2019, ApJ, 873, 118

Wechsler R. H., Bullock J. S., Primack J. R., Kravtsov A. V., Dekel A., 2002, ApJ, 568, 52

Wegg C., Gerhard O., Bieth M., 2019, MNRAS, 485, 3296

Welker C., Dubois Y., Pichon C., Devriendt J., Chisari E. N., 2015, preprint (arXiv:1512.00400)

White S. D. M., Frenk C. S., 1991, ApJ, 379, 52

White S. D. M., Rees M. J., 1978, MNRAS, 183, 341

Xue X. X. et al., 2008, ApJ, 684, 1143

Yniguez B., Garrison-Kimmel S., Boylan-Kolchin M., Bullock J. S., 2014, MNRAS, 439, 73

Zavala J., Frenk C. S., 2019, Galaxies, 7, 81

APPENDIX A: HALO AND GALAXY MASS ACCRETION RATES

Fig. A1 shows the mass growth history of the DM halo and of the central galaxy in the five MW analogues studied in Section 4. The central galaxies have assembled most of their mass by $z = 1$ (except MW1 and MW3 which have a slightly later formation time), after which they experience only a modest growth in stellar mass.

It is interesting to contrast Fig. A1 with the changes in galaxy and halo orientation shown in Fig. 10. The orientation of the central galaxies can vary considerably during the phase of rapid stellar growth ($z > 1$); however, at later times, when the mass growth is slower, the orientation remains nearly constant. In contrast, the orientation of the DM haloes can vary significantly even at $z < 1$ when their growth rate has slowed down.
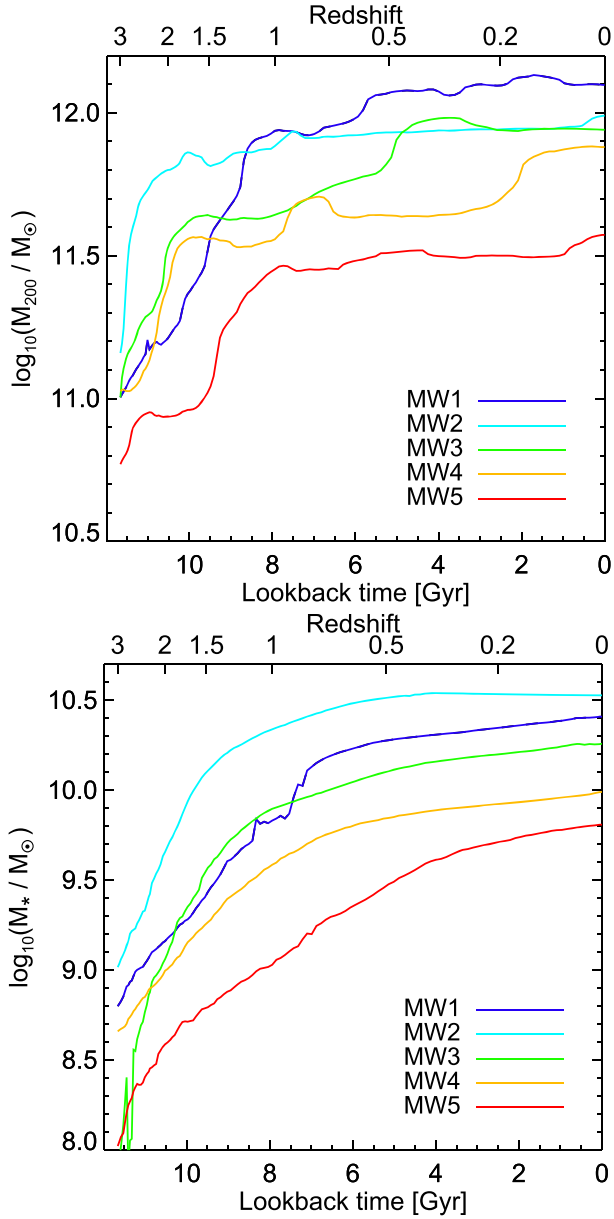
Figure A1. The mass assembly history of the DM halo (top panel) and central galaxy (bottom panel) of the five MW analogues studied in detail in this paper.

APPENDIX B: THE ORBITS OF LMC ANALOGUES

Fig. B1 shows the orbits of the three LMC mass satellites we found in our sample of analogues of the MW bright satellite population. In two of the systems, MW1 and MW3, the LMC mass satellite has just passed its second pericentre, while in MW4 the massive satellite has just passed its first pericentre.

It is instructive to compare the accretion times of the LMC analogues, that is the time when they first crossed the host halo radius, with the time when the host experienced its last large change in orientation (see Fig. 10). The three LMC mass satellites were accreted 6, 5.5, and 3 Gyr ago, while their host haloes retained a roughly constant orientation (i.e. $\cos\theta > 0.8$ in the bottom panel of Fig. 10) from 8, 5, and 4 Gyr ago, respectively. Thus, the accretion of the LMC mass satellite occurred around the same time as the last major reorientation of their MW mass host halo.
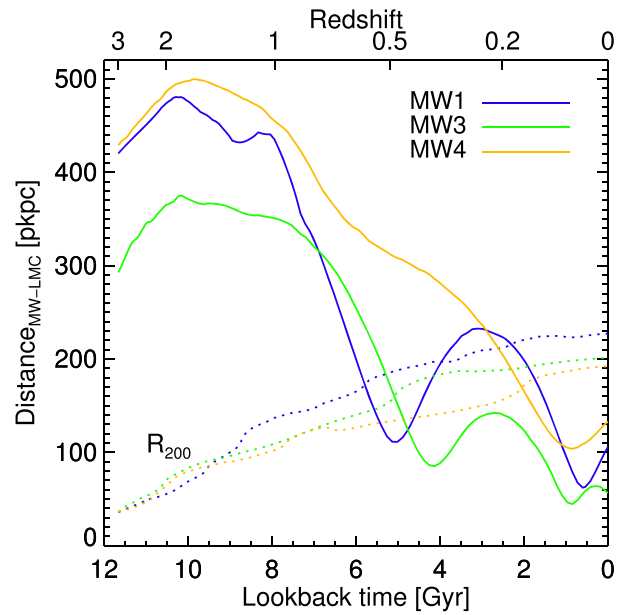

Figure B1. The distance between the LMC mass dwarf and the progenitor of the $z = 0$ MW mass host halo. The solid lines correspond to each of the three MW analogues that contain an LMC mass satellite. The dotted lines show the radius, R_{200}, of each of the three host haloes.

This paper has been typeset from a TeX/LaTeX file prepared by the author.